Journal of Catalysis **185,** 43–57 (1999)
Article ID jcat.1998.2347, available online at http://www.idealibrary.com on IDEAL®

Coprecipitated $CuO–MnO_x$ Catalysts for Low-Temperature CO–NO and $CO–NO–O_2$ Reactions

Ivanka Spassova, Mariana Khristova, Dimitar Panayotov, and Dimitar Mehandjiev[1]

Institute of General and Inorganic Chemistry, Bulgarian Academy of Sciences, 1113 Sofia, Bulgaria

Received June 11, 1998; revised September 17, 1998; accepted November 9, 1998

The activity of the mixed copper–manganese oxides $CuO–MnO_x$ ($1.5 < x < 2$), obtained by coprecipitation and activated at 300°C, has been studied for CO–NO and $CO–NO–O_2$ reactions. As shown by magnetic susceptibility data, X-ray diffraction, FTIR spectra, and catalytic tests, an interaction between CuO and MnO_x with formation of a disordered mixed oxide with a spinel-like structure is the cause of the high activity of $CuO–MnO_x$ samples.

At ambient temperature (25°C) both adsorption and interaction of CO and NO become more intense with increasing atomic fraction of copper content Cu/Cu + Mn up to 0.53 (catalyst C5M5). For the most active sample C5M5, the degree of NO conversion to N_2 attained with a $CO + NO + O_2 + Ar$ mixture is almost the same as that obtained with a $CO + NO + Ar$ mixture. A Langmuir–Hinshelwood mechanism is proposed for both (CO–NO and $CO–NO_2$) interactions at ambient temperature.

With increasing temperature under the conditions of a $CO + NO + Ar$ mixture, reduction of the catalyst surface starts. This leads in turn to depression of the CO–NO reaction at temperatures up to 130°C (low-temperature region) and to progressive acceleration of the CO–NO reaction at temperatures above 130°C (middle-temperature region). In the presence of oxygen (a $CO + NO + O_2 + Ar$ mixture), $CuO–MnO_x$ catalysts have an even higher activity over a wide temperature range (75–300°C).

Key Words: **NO; CO; O_2; low-temperature; reduction; nitric oxide; carbon monoxide; oxygen; copper–manganese; oxide; spinel; catalyst.**

INTRODUCTION

During the past several years the catalytic abatement of NO_x has attracted the attention of many laboratories worldwide because of stringent regulations for NO_x emissions. Transition metal oxides in addition to noble metal catalysts are of particular interest, specifically the achievement of low-temperature activity and selectivity with respect to NO reduction to N_2. Manganese oxides are of interest as catalysts because they have various types of labile oxygen that are necessary to complete a catalytic cycle. The oxidation of carbon monoxide at ambient temperature over amorphous mixed "hopcalite"-type catalysts has long been established (1) and this type of catalyst is still the general choice for respiratory protection. Formation of amorphous copper–manganese spinel is found to be crucial for ambient temperature oxidation of carbon monoxide by molecular oxygen (2–4). Amorphous $CuMn_2O_4$ has been stated to catalyze, at temperatures up to 500°C, the combustion of some organic substances, such as hydrocarbons and hydroxy-, halide- and nitrogen-containing compounds (5–7).

Reduction of NO by CO has been studied over Mn_3O_4 (8), and that by CO, H_2, and NH_3, over MnO (9) and MnO_2 (10). Activity and selectivity of pure manganese oxides (Mn_xO_y) in the SCR of NO with NH_3 have been investigated by Kapteijn *et al.* (11). Several studies have been published on the decomposition of NO over the manganese oxides MnO_2 (12), Mn_3O_4 (13), Mn_2O_3, and Mn_3O_4 (14). The decomposition of N_2O has also been studied over the manganese oxides MnO, Mn_3O_4, Mn_2O_3, and MnO_2 (15), and over manganese-containing perovskites (16). Composite manganese–cerium oxide is studied (17) for oxidation of CO and decomposition of N_2O. It is found that cerium provides oxygen to manganese oxide at low temperatures and, on the contrary, withdraws oxygen at high temperatures.

Some recent studies are directly related to the application of manganese oxides in catalyst systems that are developed for environmental pollution control. Exploratory research to develop Rh-free, "Pt-only" automotive catalysts is described in (18). Oxides of Co, Fe, Mn, Ti, and V show promising results when added as promoters or cocatalysts to Pt/SiO_2 to facilitate the reduction of NO by CO. Selective catalytic reduction (SCR) of NO has been studied (19) on a highly dispersed oxidic manganese layer over alumina. SCR of NO by decane under an oxidizing atmosphere has been carried out (20) on mechanical mixtures of sulfated zirconia with MnO_2 or $Cu_5Mn_{13}O_x$. A high reductive activity (NO reduction to N_2) is obtained as a result of combining the acid and oxidizing properties of sulfated zirconia and MnO_2 or $Cu_5Mn_{13}O_x$, respectively. Manganese oxide (MnO_x) is used (21) as a novel oxygen storage component (OSC) for NO

[1] To whom correspondence should be addressed. E-mail: metkomeh@bas.bg. Fax: (+359-2)705024.

0021-9517/99 $30.00

reduction and CO and CH_4 oxidation in natural-gas-fueled vehicles. The catalysts contain MnO_x supported on an inert $LaAlO_3$ perovskite and a noble metal component (Pd) supported on a separate high surface area lanthana stabilized Al_2O_3. The removal of NO by absorption on manganese zirconium oxide (Mn–Zr oxide) has been investigated (22) in both the presence and absence of gaseous O_2. The removal of NO appears to proceed by the oxidation of NO on the Mn sites and a subsequent absorption at the Zr sites as NO_3^- species. High surface area (90–400 m^2) manganese nodules show (23) a high catalytic activity in CO oxidation, and NO_x reduction by H_2, CO, or NH_3.

Selective catalytic reduction of NO by hydrocarbons in the presence of oxygen over copper ion-exchanged zeolites has been studied by Iwamoto *et al.* (24). Selective reduction of NO by water-soluble oxygen-containing organic compounds over CuZSM-5 zeolite is proposed by Monreuil and Shelef (25). Selective catalytic reduction of nitric oxide with ammonia (SCR) over supported vanadia catalysts has also been studied (26).

We have studied the activity of Cu–Mn spinels, both unsupported (27) and γ-Al_2O_3-supported (28), towards NO–CO and NO–CO–O_2 interactions. The unsupported spinel $CuMn_2O_4$ (27) exhibits an activity that is several times higher than that of Ni and Co manganites (MMn_2O_4, M = Cu, Ni, or Co). Maximal activity of supported Cu–Mn spinels is observed for samples with a Cu : Mn atomic ratio close to that of the stoichiometric $CuMn_2O_4$.

The activity of CuO–MnO_x catalysts is substantially dependent on the preparation method (2, 3, 29), most active being catalysts prepared by a coprecipitation procedure (29). It has also been found (3, 30) that the best low-temperature activity towards the CO–O_2 reaction might be obtained with a copper–manganese oxide catalyst thermally activated at 300°C.

The purpose of the present paper is to study the behavior of the mixed copper–manganese oxides CuO–MnO_x ($1.5 < x < 2$), obtained by coprecipitation and activated at 300°C, towards CO–NO and CO–NO–O_2 reactions. To the best of our knowlege this is the first report on low-temperature activity of amorphous CuO–MnO_x catalysts for NO reduction by CO.

EXPERIMENTAL

Preparation of Catalyst Samples

Samples of CuO–MnO_x were prepared using a coprecipitation procedure. Aqueous solutions of the nitrates (Ferak, Berlin) $Cu(NO_3)_2 \cdot 3H_2O$ (0.5 mol/liter) and $Mn(NO_3)_2 \cdot 6H_2O$ (0.5 mol/liter) were mixed in different ratios. The mixed nitrate solution was precipitated with an NaOH (Ferak, Berlin) solution under vigorous stirring until pH = 9. The resulting precipitate was then washed several times with distilled water until reading pH = 6 and allowed to stand in this medium for 18 h. After filtering, the precipitate was dried at 100°C for 4 h and calcined at 300°C for 4 h to give the final catalyst sample. Reference samples of the simple oxides CuO and MnO_x were prepared by an analogous procedure.

Physicochemical Characterisation

The copper content in the samples was determined by standard iodometry, using starch as indicator. Both copper and manganese were estimated by the EDTA method in the presence of hydroxylammonium chloride (A.r. grade) and hexamethylenetetramine (A.r. grade) using xylenol orange as indicator at pH = 6.

The catalyst samples were characterised by FTIR (Brüker, model IFS 25), X-ray powder diffraction (XRD) using Co$K\alpha$ radiation (TUR, Germany), magnetic measurements (Faraday-type magnetic balance), and BET surface area methods.

Catalytic Test

The catalytic experiments were carried out in a flow apparatus described previously (31). About 1 cm^3 of a catalyst (a 0.3–0.6 mm fraction) was placed into the reactor (quartz tube, d = 8 mm). Argon (purity 99.999% vol.) supplied by CHIMCO Vratza was used as a carrier gas at a total gas flow rate of 350 cm^3/min (space velocity 26,000 h^{-1}).

The concentrations of NO, NO_x ($NO + NO_2$), N_2O, CO, and CO_2 were continuously measured by gas analysers and the data were collected by a CSY-10 personal data station. The inlet concentration of CO was controlled by Infralyt 2106, NDIR gas analyser. The outlet concentrations of NO and CO were controlled by UNOR 5 (Maihak) and that of CO_2, by Infralyt 2106. A thermal converter was applied to NO_x ($NO + NO_2$) analysis. A Specord 75 IR spectrophotometer with a 1-m folded path gas cell (Specac) was used for determination of the outlet N_2O content. A Pye Unicam gas chromatograph with a calibrated volume sampler and a column with a molecular sieve were used for the analysis of O_2 and N_2 under steady-state conditions.

Temperature-programmed desorption (TPD) experiments were carried out on the same catalytic apparatus at a heating rate of 13°C/min in an Ar flow (350 cm^3/min).

Before a catalytic test each catalyst sample was treated for 1 h in an Ar flow at 300°C. Following the pretreatment procedure, the temperature was lowered to the desired level (e.g., to 25°C). The concentration step change Ar/CO + NO + Ar, CO + NO + Ar/CO + NO + O_2 + Ar was then enforced.

The data for steady-state activity of the catalyst samples were collected after 8 h testing under the same conditions as those of transient experiments.

The following competitive reactions take place when the mixture of $CO + NO + O_2$ is contacted with the catalyst surface:

$$2NO + 2CO \rightarrow N_2 + CO_2 \quad [1]$$

$$O_2 + 2CO \rightarrow 2CO_2. \quad [2]$$

In Ref. (32) we introduced the so-called redox index RO,

$$RO = (CO)_{inlet}/\{(NO)_{inlet} + 2(O_2)_{inlet}\}, \quad [3]$$

to describe the deviation of a gas flow composition ($CO + NO + Ar$ or $CO + NO + O_2 + Ar$) from the stoichiometric one ($RO = 1$) that corresponds to the full interaction of the reductant CO with the oxidants NO and O_2 to form N_2 and CO_2 according to Eqs. [1] and [2].

RESULTS AND DISCUSSION

Chemical Analysis, Surface Area, and Magnetic Susceptibility

The catalyst samples, CuO–MnO_x, were obtained under different copper–manganese ratios. The data on metal content, specific surface area, and magnetic susceptibility are shown in Table 1. The CuO–MnO_x samples are denoted as C1M9, C3M7, C5M5, C7M3, and C9M1 according to their atomic fraction of copper content ($Cu/Cu + Mn$). The assignments C10 and M10 are used for the reference samples of CuO and MnO_x, respectively.

A volcano-type relationship between the BET surface area of the CuO–MnO_x catalysts and their atomic fraction of copper content is observed. The surface area gradually increases and has a maximum at $Cu/Cu + Mn = 0.53$, with C5M5 having an area 4 times higher than that of the MnO_x sample. The incorporation of copper into the matrix of the MnO_x sample also leads to a sharp increase in the magnetic susceptibility of the catalyst samples. According to Selwood (33), this increase in magnetic susceptibility is due to the valence induction effect of the host metal oxide on the incorporated oxide. According to Kanungo (2), during the incorporation of a small quantity of copper, the metal ions interchange their coordination sites, which leads to an unequal charge distribution and an increase in metal–oxygen bond lengths of both oxides along the distortion axes (2). We suggest that incorporation of copper ions into the lattice of MnO_x would alter the exchange interaction. For this reason, an increase in magnetic susceptibility and specific surface area (2) of the oxides is observed with the transition from MnO_x to C1M9. On further increase of copper content in the catalysts, both Mn and Cu gradually shift to their regular coordination sites and, as a consequence, the magnetic susceptibility decreases again.

TABLE 1

Chemical Analysis, BET Surfaces Area and Mass Magnetic Susceptibility

Sample	Cu (at%)	Mn (at%)	Cu/Cu + Mn (a.u.)	S (BET) ($m^2\ g^{-1}$)	χ (EMU/g 10^6)
MnO_x	—	0.64	—	29	34.3
C1M9	0.14	1.10	0.11	49	56.8
C3M7	0.38	0.84	0.31	77	47.1
C5M5	0.61	0.54	0.53	128	35.5
C7M3	0.84	0.28	0.75	105	20.8
C9M1	1.09	0.13	0.89	48	9.9
CuO	0.76	—	—	5	—

X-Ray Powder Diffraction Pattern

XRD patterns of as-prepared MnO_x, CuO–MnO_x, and CuO catalysts (finally calcined in air for 4 h at 300°C) indicate X-ray amorphous samples. The FTIR spectra of these as-prepared samples are shown in the next section. We carried out an additional prolonged calcination of the samples for a total time of 160 h under the same conditions (300°C, in air). A certain crystallization of the samples was evident after the first 90 h of calcination by the appearance of very broad and low intensity lines. Table 2 shows the effect of prolonged calcination (160 h) on the X-ray diffraction patterns of CuO–MnO_x samples.

The data in Table 2 (concerning 160-h treated samples) reveal that addition of a small fraction of copper (C1M9, $Cu/Cu + Mn = 0.11$) leads to a substantial change in the host MnO_x. A series of lines disappear and/or shift to another position. With increasing copper content, the presence of a Cu–Mn spinel is observed with samples C3M7 and C5M5. With further addition of copper, new lines for CuO appear in addition to the lines corresponding to the spinel.

FTIR Spectra

The FTIR spectra (800–400 cm^{-1}) of as-prepared MnO_x and CuO are presented in Fig. 1a, and those of the mixed oxide samples CuO–MnO_x are shown in Fig. 1b. Spectra of analytical grade commercial CuO (Ferak, Berlin) and a sample of Cu–Mn oxide spinel obtained in Ref. (34) are also shown in Fig. 1. The FTIR spectra of samples treated for a long time in air at 300°C do not differ substantially from those of the as-prepared samples. Only the background absorption of treated samples is less pronounced.

It is not possible to make definite assignments of bands in this state of the phase due to the lack of a definite crystal structure of the CuO–MnO_x samples. Kanungo (2) has studied thoroughly the structure of some MnO_x–CuO mixed oxides prepared by thermal decomposition of carbonates (coprecipitated from a mixed nitrate solution by ammonium carbonate) and by thermal decomposition of nitrates. The

TABLE 2

X-Ray Powder Diffraction Patterns of CuO–MnO_x Catalysts after Prolonged Calcination (160 h, 300°C, in Air)

γMn_2O_3 6-0540[a]	γMnO_2 14-644	C1M9	C3M7	C5M5	C7M3	C9M1	CuO 5-0661	$CuMn_2O_4$ Ref. (3)	$Cu_{1.2}Mn_{1.8}O_4$ 35-1029	$Cu_{1.5}Mn_{1.5}O_4$ 35-1172
4.93 w		4.82 w	4.82 m	4.82 w	4.79 w	4.80 w		4.82 (6.1)	4.81 vw	4.79 vw
	3.96 vs	4.03 w	4.01 w							
3.75 w				3.75 w						
		3.09 vw	2.93 m	2.93 w	2.93 w	2.92 vw		2.96 (46)	2.95 w	2.937 w
		2.89 w								
		2.82 w								
2.77 s		2.78 s								
					2.73 w	2.73 w	2.751 w			
	2.60 s						2.53 m			
2.52 vs			2.49 vs	2.49 vs	2.50 vs	2.50 vs	2.523 vs	2.52 (122)	2.515 vs	2.495 vs
		2.46 s	2.46 s							
	2.42 vs	2.43 s		2.39 w	2.38 w	2.38 vw		2.41 (4.9)	2.407 vw	2.39 vw
	2.32 s	2.32 m	2.32 w				2.323 s			
				2.31 w	2.31 s	2.31 s	2.312 w			
2.22 w	2.12 s	2.19 w	2.17 w	2.20 w	2.23 vw					
	2.05 m		2.07 w	2.07 w	2.06 w	2.06 w		2.08 (17)	2.084 w	2.064 w
						1.96 vw	1.959 vw			
1.86 w		1.87 s	1.86 w		1.87 w	1.86 m	1.866 w			
				1.79 vw			1.778 vvw			
1.72 s		1.69 w	1.69 w	1.69 w	1.69 vw	1.71 w	1.714 vw	1.70 (16)	1.701 vw	1.689 vw
	1.637 s	1.65 w								
	1.605 ms	1.59 s	1.59 m	1.59 m	1.59 m	1.58 mw	1.581 w	1.60 (49)	1.604 w	1.592 m
					1.50 w	1.50 m	1.505 mw			
	1.486 w			1.48 vw						
1.45 m			1.46 w	1.46 m	1.46 m	1.46 w		1.47 (54)	1.473 m	1.458 m
	1.422 ms	1.43 w					1.418 w			
		1.41 m	1.41 w		1.41 w	1.41 mw	1.41 w			1.398 vvw
1.38 vw	1.362 m				1.39 w	1.37 mw	1.375 w			
	1.306 w					1.31 vw		1.31 (49)	1.318 vw	
								1.27 (24)	1.271 vw	
						1.26 mw	1.262 w			1.262 vw
								1.20 (2.4)		

Note. s, strong; m, medium; w, weak; v, very.

[a] Data taken from JSPDS PDF, reference numbers are given.

IR spectra of the samples obtained in this work resemble the spectra of samples prepared by thermal decomposition of nitrates in Ref. (2).

In Ref. (2) the bands of β-MnO_2 (pyrolusite) are tentatively assigned according to Farmer (35) as follows: 720 cm^{-1} (A_{2u}), 615 cm^{-1} (E_u^3), 400 cm^{-1} (E_u^2), 340 cm^{-1} (E_u^1), and 530 cm^{-1} (B_u^1). The spectrum of the MnO_x sample (Fig. 1a-1) has bands at close positions: 720, 634, 530, and 400 cm^{-1}. The sharp band at 668 cm^{-1} is analogous to that appearing in the spectra of β-MnO_2 (Ref. (2)) at 675 cm^{-1}. Incorporation of about 11 at% of copper (sample C1M9) shifts the peak at 634 to 618 cm^{-1}, a new broad band appearing around 580 cm^{-1}. This indicates possible displacement of Mn^{4+} from the octahedral site by Cu^{2+}, which results in considerable distortion or disorder in the host lattice, as explained by Kanungo (2). On further addition of copper (C3M7), the band at 618 cm^{-1} decreases in intensity. At 61 at% of copper (C5M5) both bands, at 618 and 530 cm^{-1}, disappear and a very broad band emerges around 545 cm^{-1}. The bands below 450 cm^{-1} gradually decrease in intensity. These changes indicate complete collapse of the structure and this continues up to 84 at% of copper. It is plausible that not only Mn^{4+} and Cu^{2+} interchange their coordination with respect to oxygen but also some incipient formation of a solid solution takes place during the precipitation. The C9M1 shows three well-resolved bands at 608, 509, and 440 cm^{-1}. These bands differ in both position and intensity from those observed for sample C10 (Fig. 1b-2, CuO prepared by the same procedure as that used for the CuO–MnO_x samples). The spectrum of sample C10 (CuO) is very close to that shown in Ref. (2) for CuO. However, the spectrum of the catalyst C9M1 is very close to that obtained for CuO powder and resembles that of the Cu–Mn spinel (Fig. 1b-3 and -4). Therefore, the FTIR spectra of catalyst C9M1 together with the XRD pattern (of a 160-h treated sample) indicate the presence of a mixture of CuO

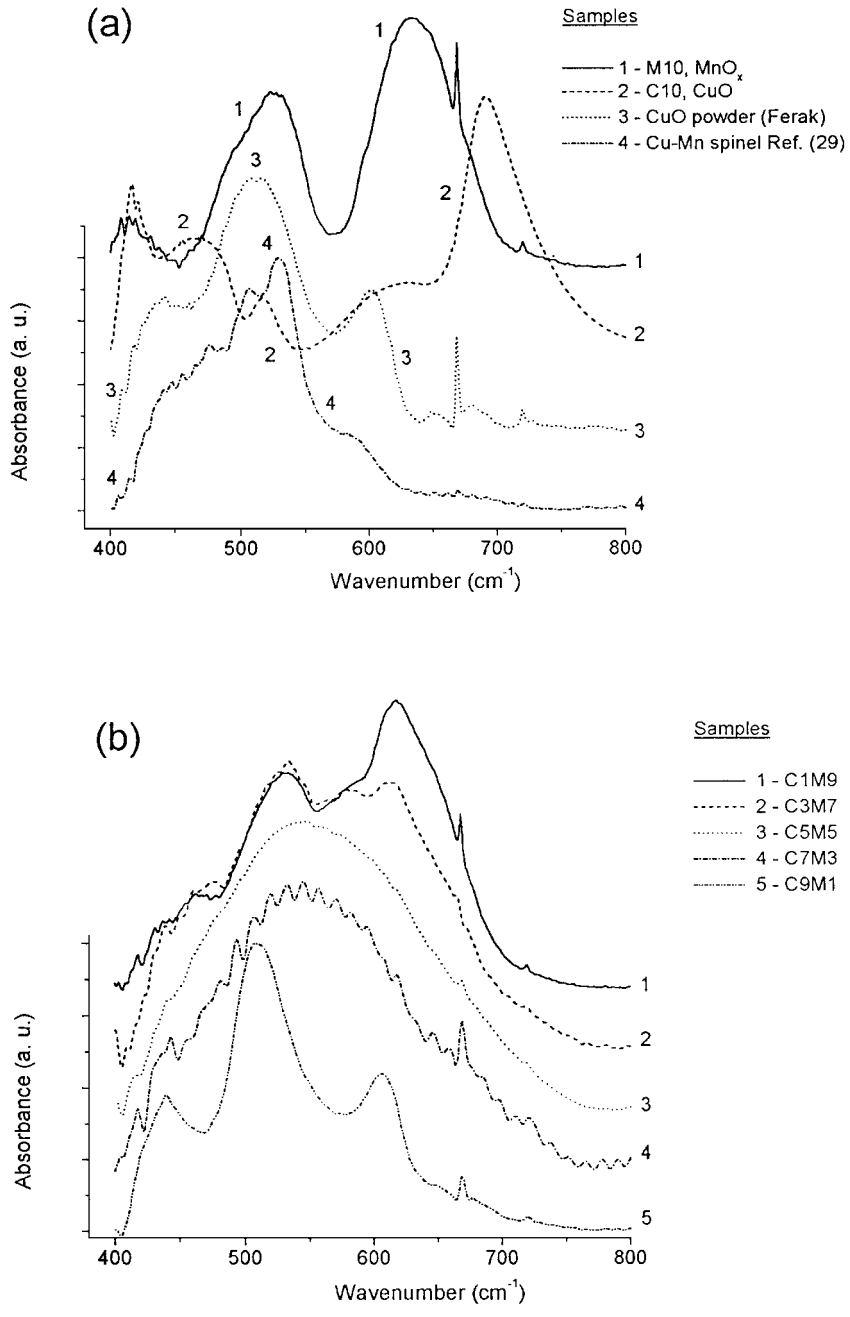

FIG. 1. FTIR spectra of as-prepared samples of (a) MnO_x, CuO; (b) CuO–MnO_x. Spectra of CuO powder (Ferak, Berlin) and Cu–Mn spinel (Ref. (29)) are given for comparison.

and a highly disordered spinel phase. The band at 720 cm^{-1} observed for the host MnO_x sample is present in the spectra of all CuO–MnO_x samples.

The broadening of IR bands with increasing copper content of the CuO–MnO_x samples could be explained in terms of Farmer's concept (35) about the IR spectra of substituted oxides. According to Farmer, when the vibration frequencies of a substituent ion and its coordinated oxygen lie within or close to those of the host oxide, the sharper bands of the pure oxides are considerably broadened. On other hand, the observed shift of the absorption bands to lower frequencies is due to the increase in metal–oxygen bond length. It is well known that in the vibrational spectrum the value of the wavenumber is directly proportional to the force constant of the bond and, hence, it increases with the increase in valence and decreases with the increase in coordination number, i.e., in bond length. The increase in the metal–oxygen bond length after addition of copper is also

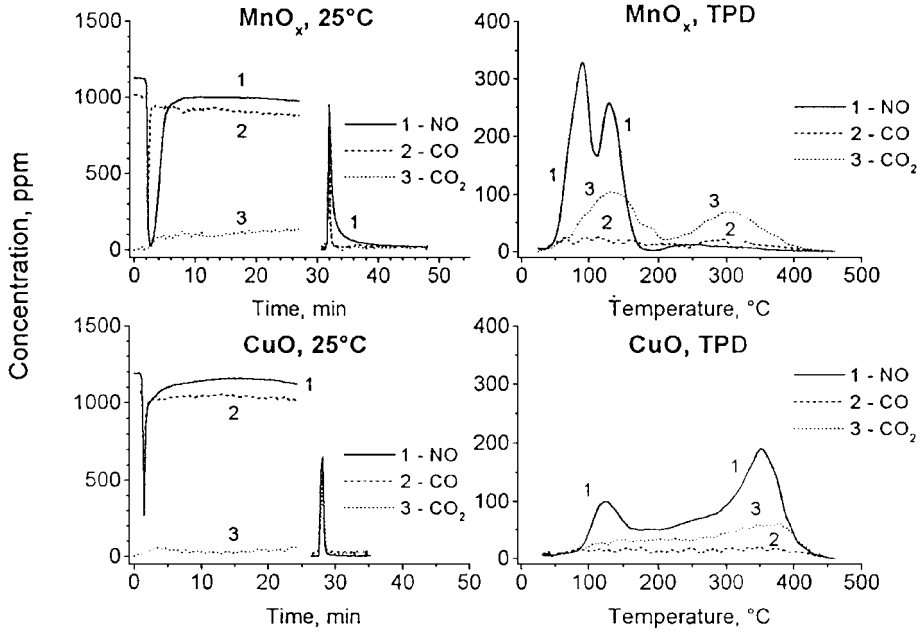

FIG. 2. Activity of MnO_x and CuO samples at ambient temperature (25°C). Transient responses of NO, CO, and CO_2 obtained during Ar/CO + NO + Ar/Ar concentration step changes, and temperature-programmed desorption (TPD) experiments.

supported by the increase in magnetic susceptibility of the CuO–MnO_x system discussed above.

Ambient Temperature Activity Towards CO–NO and CO–NO–O_2 Interactions

MnO_x and CuO catalysts. The activity of the MnO_x and CuO samples at ambient temperature (25°C) is studied towards CO–NO interaction. Following the pretreatment procedure (300°C, Ar flow) the temperature is lowered to 25°C and the concentration step change Ar/CO + NO + Ar is enforced. After about 30 min of reaction time (in a CO + NO + Ar mixture), the Ar flow is switched back and the isothermal desorption of reaction gases is followed. For both catalysts the CO responses (Fig. 2, left-hand side, curves 2) are of an instantaneous type, while monotonous responses are observed for CO_2 (Fig. 2, left-hand side, curves 3). In the case of MnO_x, a delay is registered for the response of NO, indicating the adsorption of NO on the catalyst surface. The isothermal desorption actually shows that NO is reversibly adsorbed on the surface of MnO_x. The attained conversions of CO and NO at this low temperature are fairly low (3–5%).

The data from TPD experiments (Fig. 2, right-hand side) show that both oxides differ clearly by their reactivity towards NO and CO_2. In the case of MnO_x, two peaks with close T_{max}^{NO} are observed, i.e., $T_1^{NO} = 86°C$ and $T_2^{NO} = 132°C$. The TPD spectra of NO in the case of CuO may be approximated by four Gaussians, the first and the last of which differ in T_{max} by more than 220°C, i.e., $T_1^{NO} = 125°C$ and $T_4^{NO} = 357°C$, respectively. This implies that the active sites on the CuO sample are more heterogeneously distributed by the activation energy of NO adsorption than are those on MnO_x.

CuO–MnO_x catalyst system. The catalytic experiments at ambient temperature carried out with the CuO–MnO_x catalysts comprise the Ar/CO + NO + Ar/CO + NO + O_2 + Ar/Ar reaction stages. The CuO–MnO_x catalysts are remarkably more active than are simple oxides towards the CO–NO interaction, as shown by the steady-state data in Table 3.

Incorporation of 11 at% of copper into MnO_x (sample C1M9, Cu/Cu + Mn = 0.11) increases the conversion of NO from 3–5 to 13%. On further addition of copper, the activity of CuO–MnO_x catalysts rises sharply and is about 60–70% for samples with an atomic fraction of copper content (Cu/Cu + Mn) around 0.3–0.7. In Fig. 3, the transient responses tracing this interaction are presented.

The instantaneous responses for CO_2 and the material balance for the consumption of CO and NO indicate that CO interacts first with the oxygen from the catalyst surfaces during the initial transient period. The delayed responses of NO and the corresponding desorption curves indicate the adsorption of NO on the catalyst surfaces. The reactive oxygen during the initial transient period comes from the catalyst surfaces. After depletion of this "excess oxygen," reduction of NO starts. A coincidence between CO and NO responses is observed for more active catalysts (Fig. 3, C7M3). Simultaneous adsorption of CO and NO occurs with production of CO_2 (gas chromatographic (GCh) analysis of N_2 during the transient period was impossible).

TABLE 3

Activity of CuO–MnO_x Catalysts towards CO–NO and CO–NO–O_2 Interactions at Ambient Temperature (25°C)

Catalyst sample	Steady-state conversions attained under the conditions of gas mixtures						Isothermal desorption Ar (10 min)
	CO + NO + Ar		CO + NO + O_2 + Ar				
	NO/N_2 (%)	CO/CO_2 (%)	$NO_{(total)}$ (%)	NO/N_2 (%)	CO/CO_2 (%)	O_2 (%)	NO (μmol/m^2 g)
C1M9	13	16	39	7	15	83	0.44
C3M7	61	65	57	24	54	100	0.38
C5M5	66	70	98	58	96	100	0.37
C7M3	76	80	65	24	58	100	0.23
C9M1	9	13	35	4	12	92	0.42

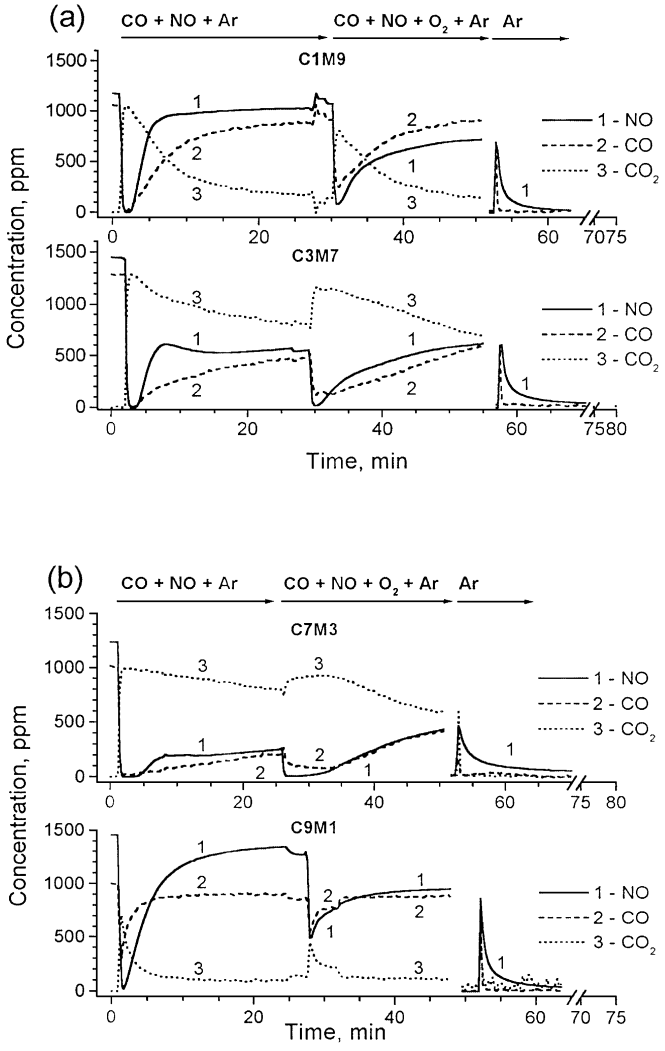

FIG. 3. Activity of CuO–MnO_x catalysts at ambient temperature (25°C): (a) C1M9 and C3M7; (b) C7M3 and C9M1. Transient responses of NO, CO, and CO_2 obtained during Ar/CO + NO + Ar/CO + NO + O_2 + Ar/Ar concentration step changes.

When added to the gas mixture, (CO + NO + O_2 + Ar stage (Fig. 3)), oxygen does not inhibit the surfaces of CuO–MnO_x catalysts towards the CO–NO interaction, as is the case with CuO (36) and Mn_3O_4 (8). Initially oxygen has some positive effect on the CO–NO reaction. However, gradual deactivation of the surfaces of CuO–MnO_x samples with time is observed. The overshoot type of the CO_2 response curves implies that the slow regeneration of active sites (37) may be the reason for this deactivation, i.e., the rate limiting step could be related to the slow desorption of the reaction product CO_2.

The data in Table 3 show that with all CuO–MnO_x catalysts the steady-state degree of total conversion of NO is higher than that of NO conversion to N_2. At the same time, oxygen is almost fully reacted and the degree of CO conversion to CO_2 is higher than that of NO to N_2. As shown by NO_x/NO analyses, fast homogeneous gas-phase oxidation of NO to NO_2 occurs at ambient temperature under the conditions of a CO + NO + O_2 + Ar mixture. The difference $NO_{(total)} - NO/N_2$ (NO converted to N_2, Table 3) corresponds to the conversion of NO to NO_2 as measured by NO_x/NO analyses. Thus, the NO_2 formed reacts with CO to give N_2. The material balance for the consumption of CO, NO, NO_x, and O_2 and the production of CO_2 and N_2 under steady-state conditions may be described correctly by the following balance equations:

$$2NO + O_2 \rightarrow 2NO_2 \quad [4]$$

$$2NO_2 + 4CO \rightarrow 4CO_2 + N_2. \quad [5]$$

For the most active sample C5M5 the steady-state degree of NO conversion to N_2 (Table 3) attained after about 25 min with CO + NO + O_2 + Ar is slightly lower than that with a CO + NO + Ar mixture. In the cases of less active catalysts (C1M9 and C9M1), NO is mostly consumed by the NO–O_2 interaction.

Kapteijn *et al.* (38) have found that NO interacts very weakly with the surface of manganese oxide supported on

alumina (2–8.4 wt% Mn). Strongly bonded oxidized species are formed in the presence of oxygen, resulting in NO_2, nitrito, and nitrate groups. These species decompose, giving back NO gas. Hence, oxygen can oxidize gas-phase NO to NO_2 as well as the catalyst surface, thus favoring NO adsorption.

TPD spectra of NO and CO_2 after CO–NO–O_2 interaction on CuO–MnO_x catalysts. After isothermal desorption following the CO + NO + O_2 + Ar experiments, TPD was carried out. With all catalysts the TPD spectra of CO were barely discernible; i.e., a very low surface coverage by CO was found. The TPD spectra of NO and CO_2 obtained with some of the catalysts are presented in Fig. 4.

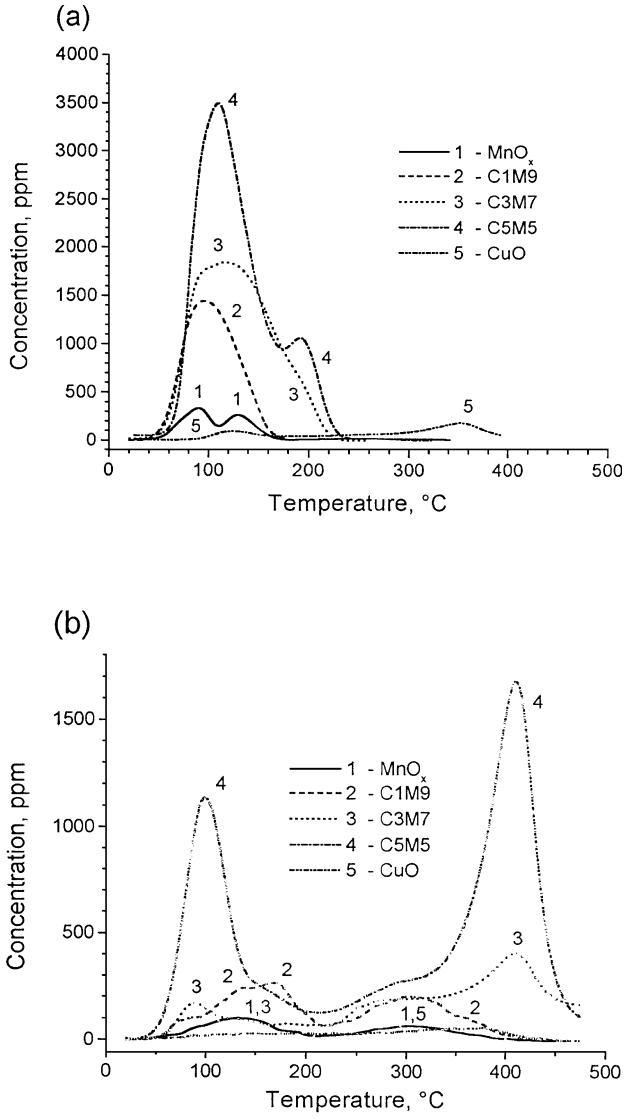

FIG. 4. Temperature-programmed desorption (TPD) spectra of NO (a) and CO_2 (b) obtained after interaction of catalysts with CO + NO + Ar and CO + NO + O_2 + Ar gas mixtures at ambient temperature (25°C).

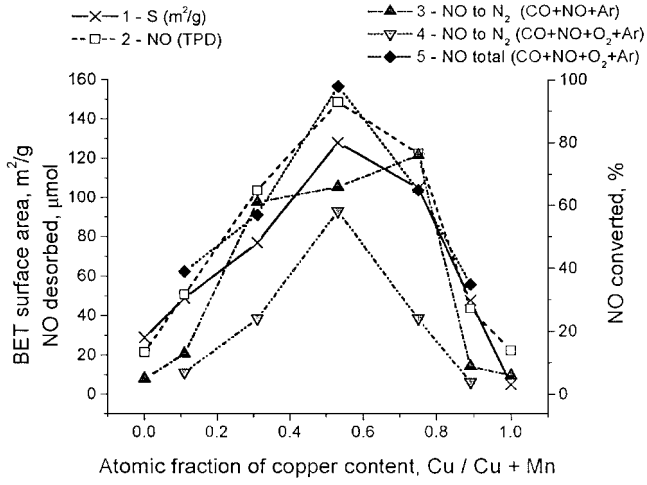

FIG. 5. Dependence of specific surface area, steady-state degree of NO conversion (total and to N_2), and amount of desorbed NO on atomic fraction of copper content (Cu/Cu + Mn) of CuO–MnO_x catalysts.

The TPD spectrum of NO observed with the C1M9 catalyst (Fig. 4a, curve 2) may be approximated by two Gaussians with T_{max}, i.e., $T_1^{NO} = 86°C$ and $T_2^{NO} = 132°C$. These maxima coincide with those obtained with MnO_x (Fig. 4a, curve 1). In the cases of C3M7 and C5M5, a new peak appears at T_{max} around 190°C. The peak is more intense with C5M5, which is the most active catalyst.

It is logical to suppose that a relation could exist between the attained degree of NO conversion during the CO + NO + O_2 + Ar stage and the amount of NO desorbed after this stage. As Fig. 5 shows, a volcano-type curve is observed for the dependence of the steady-state degree of NO conversion (total and to N_2) on the Cu/Cu + Mn ratio. This is also valid for the dependence of the amount of desorbed NO on the Cu/Cu + Mn ratio. An analogous volcano-type curve is observed with the S_{BET} vs Cu/Cu + Mn dependence. Hence, it may be deduced that the desorption of NO originates from the active sites on the catalyst surface for CO–NO and CO–NO–O_2 reactions. The number of active sites is proportional to the specific surface area of the catalysts and has a volcano-type dependence on the atomic fraction of their copper content (Cu/Cu + Mn). The maximum activity of the CuO–MnO_x samples (around 50 at% of copper) might be attributed to the formation of a highly disordered copper manganese spinel-like phase. It has been suggested that the charge transfer reaction $Cu^{2+} + Mn^{3+} \Leftrightarrow Cu^{+} + Mn^{4+}$ ensures the high activity of the amorphous copper–manganese spinel (having a Mn : Cu ratio of 1 : 1) in the CO + O_2 reaction (29, 39). If we plot the calculated amount of NO converted to N_2 per m^2 of surface area vs the Cu/Cu + Mn ratio, a volcano-type curve is observed with a maximum around Cu/Cu + Mn ≈ 3–7. This implies that the activity of CuO–MnO_x samples depends not only on the surface area but also on the Mn : Cu ratio of the catalysts.

With increasing copper content of the CuO–MnO_x catalysts, new peaks appear in the TPD spectra of CO_2 (Fig. 4b). These are a low-temperature peak with $T_1^{CO_2} = 98°C$ and a high-temperature peak with $T_4^{CO_2} = 410°C$. The first peak of CO_2 corresponds to the low-temperature peak of NO desorption. Hence, with increasing copper content in the CuO–MnO_x samples, two types of new active sites are formed on the catalyst surfaces. On the first type of new active sites, both the reagent (NO) and the product (CO_2) are adsorbed. During TPD, they are desorbed in the same temperature region, around 100°C. On the second type of active sites, only the product CO_2 is strongly adsorbed (desorbed above 350°C). It is the strong adsorption of CO_2 on these sites that may be the reason for the deactivation of catalysts at ambient temperature (≈25°C).

Behaviour of MnO_x and CuO Catalysts during the Thermal Activation of the CO–NO Reaction

After the TPD experiments, the temperature has been decreased to 50°C and a study of CO–NO interaction has been carried out. The same set of concentration steps of Ar/CO + NO + Ar/Ar are performed at 50, 75, 100, 130, 170, 200, 250, and 300°C. The temperature has been elevated stepwise. The catalysts MnO_x and CuO are almost not active at temperatures up to 100°C. The behaviour of both oxides in the temperature region 50–75°C is similar to that observed at ambient temperature: low outlet concentrations of N_2 and CO_2 are registered. At 100°C for MnO_x and at 170°C for CuO, intense interaction of CO with oxygen from the catalyst surface starts. The behaviour of CuO is analogous to that previously observed in this laboratory (36) and also discussed in detail by Rozovskii *et al.* (40). The behaviour of MnO_x above 100°C and that of CuO above 170°C resemble that of other simple oxides (8, 9, 36) and oxide spinels (27, 32, 41). The surface reduction leads to activation of the CO–NO reaction. High degrees of NO to N_2 conversion (up to 100%) are observed when increasing the temperature up to 300°C.

Behaviour of CuO–MnO_x Catalysts during Thermal Activation of CO–NO and CO–NO–O_2 Interactions

The study of CO–NO and CO–NO–O_2 interactions on CuO–MnO_x catalysts is carried out after the TPD experiments (shown in Fig. 4). The temperature is decreased to 50°C and the concentration steps Ar/CO + NO + Ar/CO + NO + O_2 + Ar/Ar are performed. The same experiments are carried out at 50, 75, 100, 130, 170, 200, 250, and 300°C. Some of these results are presented in Figs. 6 and 7.

Two temperature regions may be distinguished for the catalytic behaviour of CuO–MnO_x catalysts towards the CO–NO and CO–NO–O_2 interactions. In the first (low-temperature) region of 50 to 100°C, activation of the catalyst surfaces to both reactions (CO–NO and CO–NO–O_2) is observed for all CuO–MnO_x catalysts. In the second (middle-temperature) region of 130 to 300°C, the catalysts show some difference in behaviour towards the CO–NO reaction.

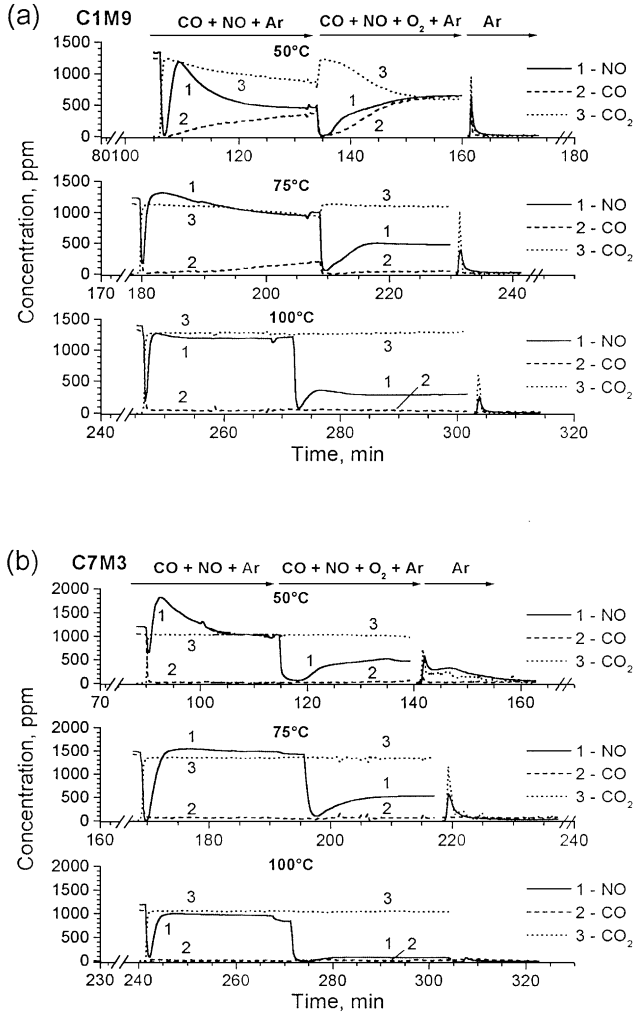

FIG. 6. Activity of some CuO–MnO_x catalysts in the low-temperature region (50–100°C). Transient responses of NO, CO, and CO_2 obtained during Ar/CO + NO + Ar/CO + NO + O_2 + Ar/Ar concentration step-changes.

Low-temperature activity of CuO–MnO_x catalysts. Figure 6 presents the results obtained at 50–100°C with catalysts C1M9 and C7M3.

At 50°C, immediately after the concentration step change Ar/CO + NO + Ar, an interaction of CO with the catalyst surface oxygen (CO–$O_{surf.}$) starts first, evolving CO_2 in the effluent gas (Fig. 6a). The extent of CO to CO_2 conversion depends on the Cu content in the CuO–MnO_x samples. For catalysts with a Cu/Cu + Mn ratio above 0.3 (C5M5, etc.), complete conversion of CO to CO_2 is observed. The CO–$O_{surf.}$ reaction leads in turn to progressive activation of the catalyst surface towards the CO–NO reaction.

It should be recalled here that after the $CO + NO + O_2$ stage at 25°C, remarkable amounts of NO are left strongly adsorbed on the catalyst surface. This NO is then desorbed in the temperature region 50–100°C during the TPD experiment (Figs. 3 and 4). Hence, it would be logical to examine the influence of preadsorbed NO on the CO–NO interaction, i.e., without inclusion of an intermediate TPD stage. The data shown in Fig. 6b for catalysts C7M3 are obtained by such a procedure (a TPD stage is not included between the concentration steps carried out at 25 and 50°C). Desorption of large amounts of NO and simultaneous complete conversion of CO to CO_2 is observed immediately after the $Ar/CO + NO + Ar$ concentration step at 50°C (Fig. 6b). It is not Ar that would initiate desorption of NO as the temperature is elevated from 25 to 50°C with Ar still passing through the reactor. Therefore, NO is displaced from the catalyst surface and thus desorbed by the adsorption of another gas (or gases) during the setting up of the $Ar/CO + NO + Ar$ concentration step. If NO is adsorbed as nitrito and/or nitro species (according to Refs. (38, 42)), then the stronger adsorption of CO and its interaction with surface oxygen (giving CO_2) are the probable reasons for the displacement of NO. Indeed, CO_2 is instantaneously evolved in the gas phase after the $Ar/CO + NO + Ar$ concentration step.

After addition of oxygen ($CO + NO + Ar/CO + NO + O_2 + Ar$ concentration step, 50°C), initial considerable consumption of NO is registered with all catalysts. Hence, the addition of oxygen to $CO + NO$ stimulates the adsorption of NO. Part of this NO is desorbed during the isothermal desorption (Fig. 6b, catalyst C7M3). More strongly adsorbed NO desorbs during the next $Ar/CO + NO + Ar$ concentration step carried out at 75°C. At 50°C, the conversion of NO to N_2 during the $CO + NO + O_2 + Ar$ stage is remarkable. For catalysts with $Cu/Cu + Mn > 0.3$ it is even higher than that observed during the $CO + NO + Ar$ stage; i.e., oxygen from the gas phase has a promoting effect on the NO to N_2 conversion.

At 75 and 100°C the extent of $CO–O_{surf.}$ interaction during the $CO + NO + Ar$ stage increases, and the NO to N_2 reduction is strongly depressed. On the contrary, during the $CO + NO + O_2 + Ar$ stage the rate of NO reduction to N_2 is enhanced. For the most active C5M5 and C7M3 catalysts, conversion degrees of NO to N_2 over 90% are attained at 100°C during the $CO + NO + O_2 + Ar$ stage. These results are remarkable, bearing in mind that under these conditions the amount of oxidants exceeds by >50% that required by the stoichiometry of the $CO–NO–O_2$ interaction (a redox potential $RO = 0.43$ is used). With all the catalysts, complete conversion of CO to CO_2 is attained at 75 and 100°C. According to the material balance for the gas phase, an additional reaction of catalyst surface reoxidation also occurs during the $CO + NO + O_2 + Ar$ stage at the expense of excess oxidants. Thus, when the gas-phase composition is cycled between the $CO + NO + Ar$ and $CO + NO + O_2 + Ar$ mixtures, the state of the catalyst surface varies between reduced and oxidised.

Therefore, during the $CO + NO + Ar$ stages an intense interaction of CO from the gas phase with the surface oxygen that causes depletion of adsorbed NO (thus depressing its adsorption and reduction) is characteristic for the CO–NO reaction in the low-temperature region. During the $CO + NO + O_2 + Ar$ stage, the gas-phase oxygen causes an enhancement of NO reduction, although oxidising conditions are realised. It is reported in the literature that the catalytic reduction of NO_2 by CO (43, 44) or by HC (45) is much faster than the NO reduction. We suggest that it is fast oxidation of NO to NO_2 followed by fast reduction of NO_2 by CO that outlines the probable reaction route for N_2 formation. This might explain the higher degrees of NO conversion to N_2 observed during the $CO + NO + O_2 + Ar$ stage as compared to the conversion detected during the $CO + NO + Ar$ stages.

Middle-temperature activity of $CuO–MnO_x$ catalysts. In the middle-temperature region (130 to 300°C) the interaction of CO with catalyst surface oxygen ($CO–O_{surf.}$) also proceeds during the $CO + NO + Ar$ stages. However, NO reduction to N_2 is not depressed as much as it is at 75 and 100°C. In the case of the catalyst C1M9 (Fig. 7a), at a temperature of 170°C and above, the surface reduction leads in turn to gradual enhancement of NO reduction to N_2.

It is the competition between the catalyst surface oxygen and NO for interaction with CO that defines the rate of N_2 production. This oxygen is accumulated on the surface during the $CO + NO + O_2 + Ar$ stages, because an excess of oxidants is applied (a redox potential $RO = 0.4–0.5$). The amount of oxygen depleted from the catalyst surface during the $CO + NO + Ar$ stage and that transferred back to the surfaces during a subsequent $CO + NO + O_2 + Ar$ stage are close (equal duration of stages is used). In the cases of the most active catalysts C5M5 and C7M3, the amounts of transferred oxygen are within the range 15–20% of monolayer surface coverage. The amount of oxygen present in one monolayer of the oxide surface has been approximated in Ref. (41) to about 10^{19} atom/m^2. For the less active catalysts C1M9, C3M7, and C9M1, the amounts of transferred oxygen are about 30–35, 20–25, and 15–20% of monolayer surface coverage, respectively.

In this temperature region, measurable steady state conversions of NO to N_2 are attained during the $CO + NO + Ar$ stages; i.e., the reduction of NO to N_2 is fast enough to compete with the $CO–O_{surf.}$ reaction. Analogous behaviour has been observed with simple oxides (36) and manganites (MMn_2O_4, M = Cu, Ni, Co) (27) and cobaltites ($Cu_xCo_{(3-x)}O_4$ (41)). However, these catalysts lose completely (CuO, (36)) or to some extent (MMn_2O_4 (27) and $Cu_xCo_{(3-x)}O_4$ (41)) their activity in NO reduction when O_2 is added to the gas phase. As may be seen in Figs. 6

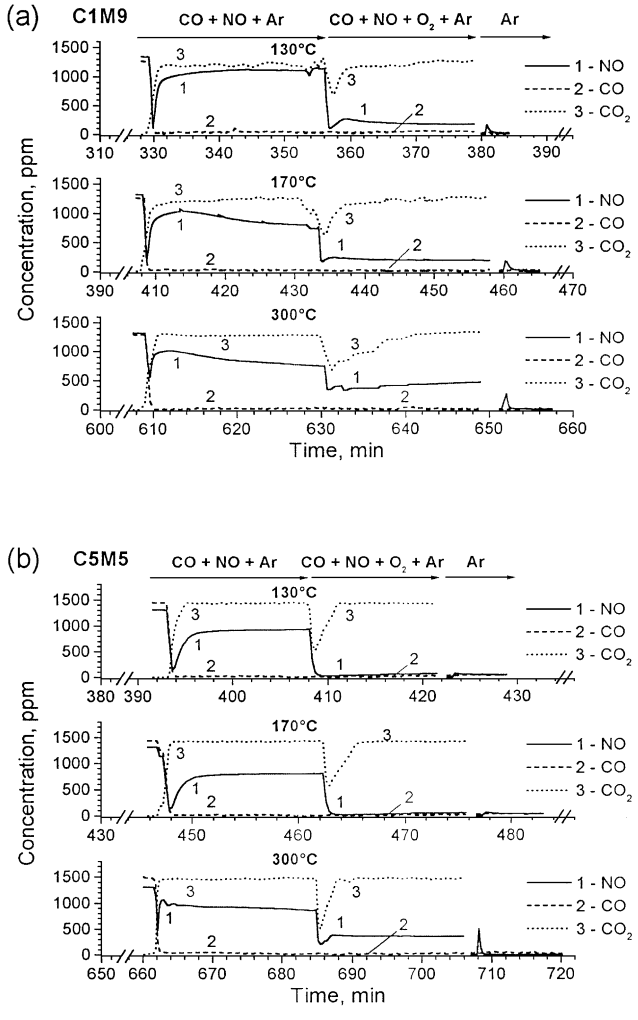

FIG. 7. Activity of some CuO–MnO_x catalysts in the middle-temperature region (130–300°C). Transient responses of NO, CO, and CO_2 obtained during concentration step changes Ar/CO + NO + Ar/CO + NO + O_2 + Ar/Ar.

and 7, CuO–MnO_x catalysts have an even higher activity in the presence of oxygen. Moreover, this behaviour of CuO–MnO_x catalysts is observed over a wide temperature range (75–300°C).

At temperatures above 200°C, some decrease in the rate of NO reduction is observed for all catalysts during the CO + NO + O_2 + Ar stages (Fig. 7). If the oxidation of NO to NO_2 and the subsequent reaction of NO_2 with CO are accepted as stages of an appropriate route for NO reduction, then the inhibition of the NO–O_2 gas-phase reaction with increasing temperature may account for the partial depression of NO reduction. It is known that the NO–O_2 reaction has a negative temperature coefficient.

The most important point here is that for all catalysts the addition of O_2 at the CO + NO + O_2 + Ar stages leads to an increase in the rate of NO reduction. Formation of NO_2 (via homogeneous or even catalytic oxidation of NO) and its subsequent interaction with CO might be suggested as key steps for the mechanism of NO reduction to N_2 on the surface of CuO–MnO_x catalysts under the oxidising conditions of the CO + NO + O_2 + Ar gas mixture. It was previously concluded by Shelef *et al.* (46) that the catalyst (H-ZSM5, Cu-ZSM5, or Cu/Al_2O_3) which has the highest activity in NO oxidation to NO_2 also has the highest activity towards NO decomposition. Using isotope labeling technique, Chang and McCarty (47) have established that NO_x reduction over Cu-ZSM5 and Co-ZSM5 proceeds via NO_2 intermediates at very low temperatures (<200°C).

Adsorption properties and activity of a C5M5 catalyst at ambient temperature. In order to gain a better understanding of the interaction of the gas phase with the surface of CuO–MnO_x catalysts, we have carried out a set of sequential stages of reaction and TPD with the most active catalyst C5M5. The reaction stages are carried out at ambient temperature with NO + Ar, CO + Ar, NO + O_2 + Ar, CO + NO + Ar, and CO + NO + O_2 + Ar gas mixtures. The results are presented in Fig. 8. The sample of catalyst C5M5 has not been withdrawn from the reactor after the experiments shown in Fig. 7; i.e., the same sample has been utilized.

The first stage of the experiments includes the interaction of a NO + Ar mixture with the surface of the used C5M5 catalyst (Fig. 8a).

The material balance shows that about 329 μmol NO are consumed during the reaction stage, 49 μmol are desorbed during the isothermal desorption stage and 169 μmol are desorbed in the TPD experiment (Fig. 8b). The two latter amounts correspond to approximately 2 and 8%, respectively, of NO surface coverage. Hence, about 111 μmol of NO consumed during the reaction stage is not registered in the TPD stage. Gas chromatographic analysis has indicated the evolution of a trace amount of N_2. However, the sensitivity of the GCh analysis has not been sufficient for evaluation of the material balance.

During the CO + Ar stage (Fig. 8c), remarkable conversion of CO to CO_2 is observed even at a low temperature (25°C). The material balance has shown that 435 μmol CO is consumed and 345 μmol CO_2 is produced. During the isothermal desorption, 18 and 13 μmol of CO and CO_2, respectively, are evolved, while 7 and 53 μmol of CO and CO_2 are desorbed during the TPD (Fig. 8d). These data show full equilibration of the amounts of consumed CO and the sum $CO_{(desorbed)} + CO_{2(produced)}$, (about 440 μmol). The amount of surface oxygen involved in the CO_2 production is 411 μmol, which corresponds to approximately 19.6% of monolayer coverage. This implies the existence of very reactive oxygen left on the surface of the C5M5 catalyst after the NO + Ar/TPD stages. The fact that both CO and CO_2 are desorbed simultaneously during the TPD stage indicates the participation of CO and surface oxygen in

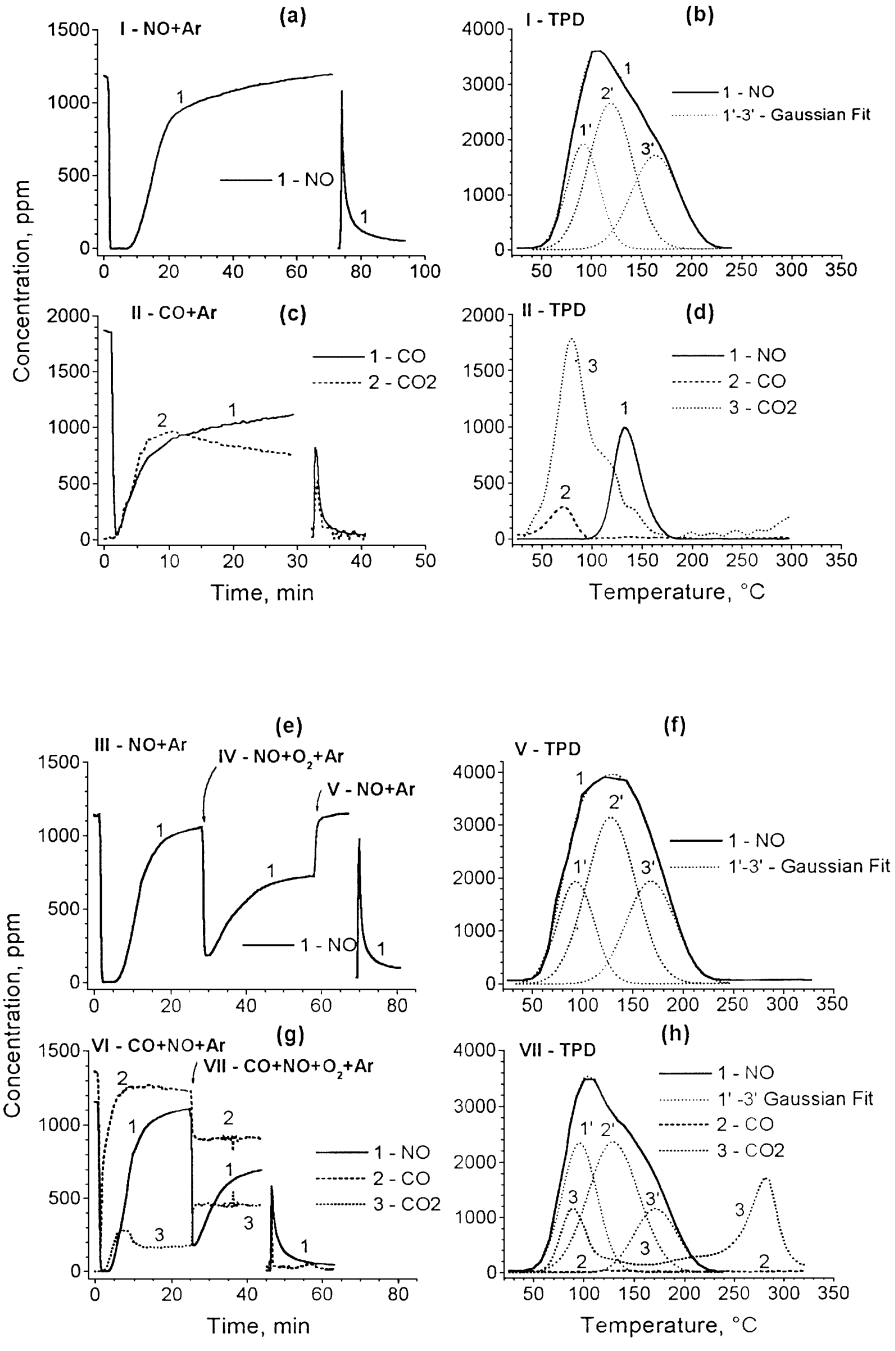

FIG. 8. Sequential reaction and TPD stages carried out with the most active catalyst C5M5. The reaction stages are performed at ambient temperature (25°C) with NO + Ar, CO + Ar, NO + O_2 + Ar, CO + NO + Ar, and CO + NO + O_2 + Ar gas mixtures. Transient responses of NO, CO, and CO_2.

the same (probably carbonate-like) surface species. These species are easily destroyed even at ambient temperature to give CO_2. Desorption of CO_2 is complete at temperatures as high as 170°C.

The subsequent stages (III–V, NO + Ar/NO + O_2 + Ar/ NO + Ar) show (Fig. 8e) some interesting features. In stage III, nitric oxide reacts with the catalyst surface in a manner analogous to that in the stage I (matching NO responses are observed). Addition of oxygen at stage IV leads to an abrupt increase in the consumption of NO. With time the outlet concentration of NO is monotonously increased. The transient response of NO could reflect a fast homogeneous NO–O_2 reaction followed by adsorption of NO_2 on the catalyst surface. In the steady state (after 20–25 min

reaction time), O_2 is completely consumed (GCh analysis) and about 30% of NO_x belong to NO_2 (NO_x/NO analysis). Hence, in the steady state NO and O_2 are stoichiometrically reacted. It has been reported that oxidation of NO by O_2 to form NO_2 is effectively catalyzed by some zeolite-based catalysts (Ref. (47), and the references therein) at a relative low temperature, e.g., ambient temperature. The TPD spectra of NO (Fig. 8f) comprise three peaks (Gaussian fit) as observed in the TPD spectra after the adsorption of NO (Fig. 8b). The T_{max} of those three peaks are practically at the same positions but the height and the area of the second peak are increased. This may be attributed to the partial reoxidation of the catalyst surface during the $NO + O_2 + Ar$ stage. The material balance for NO has shown that half of the consumed NO is left as adsorbed on the catalyst surface. As established in Ref. (46), formation of NO_2-like species, part of which is desorbed as NO, could also be suggested.

The last two reaction stages (VI and VII) comprise experiments with $CO + NO + Ar$ and $CO + NO + O_2 + Ar$ gas mixtures (Fig. 8g). In stage VI the amounts of CO reacted and CO_2 produced coincide well and show that about 54 μmol of CO are reacted with NO. Comparison of the NO response with those of CO and CO_2 shows that under these conditions NO is more strongly adsorbed on the catalyst surface than are CO and CO_2.

Addition of O_2 (stage VII) leads to precipitous changes in the concentrations of all gases. The response curves for CO and CO_2 synchronize well. Obviously, even at ambient temperature oxygen steps immediately in the interaction and the CO_2 production is sharply increased. The steady-state concentrations of CO, NO, and CO_2 (oxygen is completely consumed) and the material balance indicate that NO is oxidised to NO_2, which reacts with CO to give CO_2. The TPD spectrum of NO (Fig. 8h) is close to that observed in the stage I-TPD (Fig. 8b), i.e., after the $NO + Ar$ reaction stage I. The amount of desorbed NO in VII-TPD is about 166 μmol. The calculated (on the basis of material balance) total amount of adsorbed NO during the reaction stages VI and VII corresponds to about 145 μmol. These values for adsorbed NO are close enough to support the suggestion that NO_2 is an intermediate product of NO conversion to N_2.

Proposed reaction pathways of the mechanism of ambient temperature CO–NO and CO–NO–O_2 interactions. The foregoing data show that amorphous CuO–MnO_x oxides have much greater ability to adsorb and activate CO and NO molecules in their catalytic interaction than do the simple oxides MnO_x and CuO. In Ref. (2) it has been established that the activity of CuO–MnO_x catalysts can be correlated better with surface excess oxygen than with active (or available) oxygen which is a bulk property. This correlation is supported by the direct relationship between activity and specific surface area. In the present work, an analogous relationship is found between the ambient temperature activity of CuO–MnO_x catalysts towards NO reduction and the specific surface area. As shown by magnetic susceptibility data and XRD and FTIR spectra, an interaction between oxides with formation of a disordered mixed oxide (with probable spinel structure) is the cause for the high activity of CuO–MnO_x samples. The greatest activity of catalyst C5M5 might be attributed to the highly disordered copper–manganese spinel phase. Metal ions of different oxidation states will be created on the surface of such a disordered phase, and thus the adsorption of CO and NO will be facilitated. This is clearly shown by the correlation between the amount of desorbed NO and the activity of the catalysts (Fig. 5). It has been reported recently (48) that two types of Cu–Mn spinels, i.e., $Cu^{2+}Mn_2^{3+}O_4$ and $Cu^{+}[Cu_{0.5}^{2+}Mn_{1.5}^{4+}]O_4$, may be formed in the CuO–MnO_x oxide system. It may be suggested that a redox couple, $Cu^{2+} + Mn^{3+} \Leftrightarrow Cu^{+} + Mn^{4+}$, formed on the surface of CuO–MnO_x samples may play a certain role in the catalytic reaction mechanism of NO–CO reaction.

Yamashita and Vannice (4) have suggested that NO decomposition over Mn_2O_3 proceed via a second-order, rate determining surface reaction between NO molecules or NO-related intermediates, with retardation effects of oxygen or oxygen-related intermediates. Adsorption of NO on an active site, designated as $*$, and a Langmuir–Hinshelwood (L-H) model are proposed for NO decomposition. The suggested NO-related intermediates are NO^* or N_2O^*, where N_2O^* species are rapidly decomposed to give N_2.

In the case of CO–NO interaction on CuO–MnO_x catalysts, we have observed simultaneous adsorption of CO and NO at ambient temperature and formation of CO_2 (GCh analysis of N_2 during the transient period was impossible). The coincidence between CO and NO responses is better for more active catalysts (Fig. 3). Adsorbed CO is mainly desorbed as CO_2, and NO and CO_2 have close T_{max} around 100°C (Figs. 4 and 8f). The foregoing implies the formation of both CO-related and NO-related intermediate species for the CO–NO interaction. We have proposed (49), on the basis of IR spectra, and kinetic and TPD data, formation of a surface carbonate complex for CO adsorption and of nitro- or nitrito-like complexes for NO adsorption in order to explain the low-temperature (25–50°C) activity of the $CuCo_2O_4$ catalyst. Hence, the steps compose the path of the CO–NO reaction mechanism that occurs on the surface of CuO–MnO_x catalysts at ambient temperature. Hence, by analogy with the scheme for NO decomposition (4) it might be suggested that an L-H model would be plausible for describing the CO–NO interaction. Thus, after being formed on the catalyst surface, CO- and NO-related intermediates interact to give finally N_2 and CO_2. On less active catalysts (e.g., C1M9 and C9M1), production of CO_2

is favored via interaction of CO with surface oxygen (O^*_{cat}). Formation of an unstable intermediate surface carbonate complex via a primary and rate controlling step of CO combination with surface oxygen has been proposed by Brittan *et al.* (50) and also by Kanungo (3) for ambient temperature oxidation of CO. Formation of $Cu^{2+}(O^-)(NO)$ species is supposed as a primary step for NO decomposition on Cu-ZSM5 catalysts (47, 51).

Under addition of O_2 at ambient temperature, fast homogeneous gas-phase oxidation of NO to NO_2 occurs, as shown by NO_x/NO analysis. The data in Table 3 and NO responses observed in the CO + NO + O_2 + Ar stage (Fig. 3) imply some contribution of catalytic oxidation of NO on the catalyst surfaces as observed on other Cu-containing catalysts (46, 47). Oxygen has no strong inhibition effect on NO reduction, although oxidizing conditions are realised (redox index RO $\approx$ 0.4–0.5), as previously observed for base metal oxide catalysts (8, 27, 36, 41). Presumably, the reduction of NO_2 by CO is fast enough (43, 44) to compete with the CO–O_2 reaction. Thus, interaction between CO- and NO_2-related intermediates to produce finally N_2 and CO_2 is suggested for the CO–NO–O_2 interaction. The slow deactivation of the catalyst surfaces is most probably due to the formation of strongly held carbonates, which decompose at high temperature (above 250°C, Figs. 4 and 8f). Thus, we suggest that the L-H model can also be accepted for description of CO–NO_2 interaction at ambient temperature. With increasing temperature (from 25 to 50°C), adsorbed NO_2 decomposes with elution of NO or reacts with CO to liberate NO (Figs. 6).

The results of the present work show that effective catalysts for low-temperature CO–NO and CO–NO–O_2 reactions can be obtained on the basis of the CuO–MnO_x oxide system. Further study on the stability of these catalysts towards poisons such as water and SO_2 are now in progress.

ACKNOWLEDGMENTS

Financial support of this work from the Foundation for Scientific Investigations at the Ministry of Science and Education, Project X-621, is gratefully acknowledged. The help of Dr. D. Stoilova with the FTIR study and Dr. D. Kovacheva with the XRD analysis is greatly appreciated.

REFERENCES

1. Lamb, A. B., Bray, W. C., and Frazer, J. C., *J. Ind. Eng. Chem.* **12**, 213 (1920).
2. Kanungo, S. B., *J. Catal.* **58**, 419 (1979).
3. Kanungo, S. B., *Indian J. Chem.* **26A**, 373 (1987).
4. Hutchings, G. J., Mirzaei, A. A., Joyner, R. W., Siddiqui, M. R. H., and Taylor, S. H., *Catal. Lett.* **42**, 21 (1996).
5. Christian, J. G., and Johnson, J. E., *Int. J. Air Wat. Poll.* **9**, 1 (1965).
6. Mušick, J. K., and Williams, F. W., *Ind. Eng. Chem. Prod. Res. Dev.* **13**, 175 (1974).
7. McCabe, R. W., and Mitchell, P. J., *Ind. Eng. Chem. Prod. Res. Dev.* **23**, 196 (1984).
8. Alkhazov, T. G., Gassan-zadeh, G. Z., Osmanov, M., and Sultanov, Yu., *Kinet. Katal.* **16**, 1230 (1975).
9. Shelef, M., and Otto, K., *J. Catal.* **10**, 408 (1968).
10. Echigoya, E., Niiyama, H., and Ebitani, A., *Nippon Kagaku Kaishi*, 222 (1974).
11. Kapteijn, F., Singoredjo, L., Andreini, A., and Moulijn, J. A., *Appl. Catal. B* **3**, 173 (1994).
12. Yur'eva, T. M., Popovski, V. V., and Boreskov, G. K., *Kinet. Catal.* **6**, 941 (1965).
13. Edwards, H. E., and Harrison, R. M., *Environ. Sci. Technol.* **13**, 673 (1979).
14. Yamashita, T., and Vannice, A., *J. Catal.* **163**, 158 (1996).
15. Yamashita, T., and Vannice, A., *J. Catal.* **161**, 254 (1996).
16. Mizuno, N., Tanaka, M., and Misono, M., *J. Chem. Soc. Faraday Trans.* **88**, 91 (1992).
17. Imamura, S., Shono, M., Okamoto, N., Hamada, A., and Ishida, S., *Appl. Catal. A* **142**, 279 (1996).
18. Mergler, Y. J., Chandoesing, R., and Nieuwenhuys, B. E., *Rec. Trav. Chim. J. Roy. Neth. Chem.* **115**, 474 (1996).
19. Kijlstra, W. S., Poels, E. K., Bliek, A., Weckhuysen, B. M., and Schoonheydt, R. A., *J. Phys. Chem. B* **101**, 309 (1997).
20. Delahay, G., Coq, B., Ensuque, E., and Figueras, F., *C. R. Acad. Sci. Ser. II B* **322**, 881 (1996).
21. Chang, Y. F., and Mccarty, J. G., *Catal. Today* **30**, 163 (1996).
22. Eguchi, K., Watabe, M., Ogata, S., and Arai, H., *Bull. Chem. Soc. Jpn.* **68**, 1739 (1995).
23. Parida, K. M., Satapathy, P. K., Das, N. N., and Rao, S. B., *J. Sci. Ind. Res. India* **55**, 234 (1996).
24. Iwamoto, M., Mizuno, N., and Yahiro, H., *in* "Proceedings, 10th International Congress on Catalysis, Budapest, 1992" (L. Guczi, F. Solymosi, and P. Tetenyi, Eds.), p. 213, Akadémiai Kiadó, Budapest, 1993.
25. Monreuil, C. N., and Shelef, M., *Appl. Catal. B* **1**, L1, (1992).
26. Forzatti, P., and Lietti, L., *Heterogeneous Chem. Rev.* **3**, 33 (1996).
27. Khristova, M., Panayotov, D., and Mehandjiev, D., *in* "Prep. 7th International Symposium on Heterogeneous Catalysis," Part 2, p. 1025, Burgas, Bulgaria, 1991.
28. Panayotov, D., *React. Kinet. Catal. Lett.* **58**, 73 (1996).
29. Puckhaber, L. S., Cheung, H., Cocke, D. L., and Clearfield, A., *Solid State Ionics* **32/33**, 206 (1989).
30. Spasova, I., and Mehandjiev, D., *React. Kinet. Catal. Lett.* **58**, 57 (1996).
31. Panayotov, D., Khristova, M., and Mehandjiev, D., *Appl. Catal.* **34**, 48 (1987).
32. Panayotov, D., and Mehandjiev, D., *in* "Proceedings, IVth International Symposium on Heterogeneous Catalysis," Part 2, p. 255, Varna, Bulgaria, 1979.
33. Selwood, P. W., *in* "Advances in Catalysis" (W. G. Frankenburg, E. K. Rideal, and V. I. Komarewasky, Eds.), p. 52. Academic Press, New York, 1952.
34. Koleva, V., Stoilova, D., and Mehandjiev, D., *J. Solid State Chem.* **133**, 416 (1997).
35. Farmer, V. C., *in* "Infrared Spectra of Minerals" (V. C. Farmer, Ed.), p. 186. Mineralogical Society, London, 1974.
36. Panayotov, D., and Mehandjiev, D., *in* "Proceedings, 10th International Congress on Catalysis, Budapest, 1992" (L. Guczi, F. Solymosi, and P. Tetenyi, Eds.), p. 263. Akadémiai Kladó, Budapest, 1993.
37. Kobayashi, M., *Chem. Eng. Sci.* **37**, 393 (1982).
38. Kapteijn, F., Singoredjo, L., Vandriel, M., Andreini, A., Moulijn, J. A., Ramis, G., and Busca, G., *J. Catal.* **150**, 105 (1994).
39. Veprek, S., Cocke, D. L., Kehl, S., and Oswald, H. R., *J. Catal.* **100**, 250 (1986).
40. Rozovskii, A., Sticenko, V., and Tretjakov, V., *Kinet. Catal.* **14**, 1082 (1973).

41. Panayotov, D., Khristova, M., and Mehandjiev, D., *J. Catal.* **156**, 219 (1995).
42. London, J. W., and Bell, A. T., *J. Catal.* **31**, 96 (1973).
43. Gura, Yu., and Yuzefovich, G., *Cataliz i Catalizatori* **14**, 8 (1976).
44. Gassan-zadeh, G. Z., Mukherjee, T. K., and Alkhazov, T. G., *React. Kinet. Catal. Lett.* **12**, 525 (1979).
45. Armor, J. N., *Appl. Catal. B* **1**, 221 (1992).
46. Shelef, M., Montreuil, C. N., and Jen., H. W., *Catal. Lett.* **26**, 277 (1994).
47. Chang, Y., and McCarty, J. G., *J. Catal.* **165**, 1 (1997).
48. Koleva, V., Stoilova, D., and Mehandjiev, D., *J. Solid State Chem*. **133**, 416 (1997).
49. Panayotov, D., Matyshak, V., Sklyarov, A., Vlasenko, A., and Mehandjiev, D., *Appl. Catal.* **24**, 37 (1986).
50. Brittan, M. A., Bliss, M. A., and Walker, C. A., *A.I.Ch.E.J.* **16**, 305 (1970).
51. Aylor, A. W., Larsen, S. C., Reimer, J. A., and Bell, A. T., *J. Catal.* **157**, 592 (1995).